Journal of Crystal Growth **23** (1974) 113–120 © *North-Holland Publishing Co.*

GROWTH AND MICROSTRUCTURAL CONTROL OF SINGLE CRYSTAL CUPROUS OXIDE Cu_2O

R. D. SCHMIDT-WHITLEY* and M. MARTINEZ-CLEMENTE**

Laboratoire de Physique des Matériaux, Centre National de la Recherche Scientifique, 92190 Meudon, France

and

A. REVCOLEVSCHI

Laboratoire de Chimie Appliquée de l'Etat Solide, 94100 Vitry-sur-Seine, France

Received 10 February 1974; revised manuscript received 22 April 1974

Large single crystals of cuprous oxide, Cu_2O, have been grown by a floating zone technique using an arc-image furnace. The microstructure of the polycrystalline starting material obtained by oxidation of copper and of the single crystals grown from the melt have been investigated in detail, as well as the influence of atmosphere, solidification rate and impurity concentration. The precipitate structure inherent to the conditions of crystal growth was extremely complex, consisting of various forms of cupric oxide inclusions and aggregates of gas and cupric oxide. The microstructural changes accompanying high-temperature annealing within the cuprous oxide stability field are described. A procedure for crystal growth and treatment which minimizes the amount of defects is developed.

1. Introduction

The physical properties of cuprous oxide Cu_2O are greatly influenced by the degree of perfection of the crystalline structure, i.e. by the presence of dislocations, grain boundaries, solute atoms, precipitates, or departures from stoichiometry. It is thus imperious that data on the basic electrical, magnetic, optical or mechanical properties should be evaluated from single crystals of controlled quality. Most of the early investigations on cuprous oxide were conducted on ill-defined polycrystalline material. Several methods for the growth of single crystals have been applied, for instance grain-growth of polycrystalline sheets[1,2]), oxidation of single crystal copper[3]), hydrothermal growth[4]), and more recently growth from the melt with[5]) and without[6,7]) a crucible. Amongst these methods, crucible-free growth of single crystals from the melt has many advantages, since it satisfies the requirements of chemical purity and makes growth of large and suitably oriented crystals possible. However, considerable confusion still exists regarding the growth conditions and the nature of the microstructural defects.

There are several difficulties encountered in preparing cuprous oxide: Cu_2O has a high chemical reactivity at temperatures above about 1000 °C both in the solid and especially in the molten state (T_m = 1125 °C in air). Added to this is the fact that at ambient temperature and atmosphere the stable phase in the system copper–oxygen is cupric oxide, CuO. The cuprite field as communicated by O'Keeffe and Moore[8]) has been corrected in the light of the phase relationships of the equilibrium diagram[9]), and recent results[10]) have been used to construct the pressure–temperature diagram of fig. 1. It can be seen that unless special precautions are taken during the cooling of cuprous oxide from the generally high temperatures at which it is prepared, certain reactions will occur. One of the obvious reactions is the surface oxidation of cuprous oxide to cupric oxide:

$$Cu_2O + \tfrac{1}{2}O_2 \rightarrow 2\,CuO. \qquad (1)$$

Solid state phase transformations within the bulk of the crystals leading to internal precipitation of CuO cannot be excluded either.

Once the surface film of CuO has been removed, it is possible to investigate the microstructure of thin specimens by optical transmission. Whilst some authors[1,11]) who studied coupons of cuprous oxide obtained by total oxidation of copper report a lack of defects even

* Present address: IRSID, Station d'Essais, 57210 Maizières-lès-Metz, France.

** On leave from the Laboratory of Electron Microscopy, Faculty of Science, University of Madrid, Madrid, Spain.

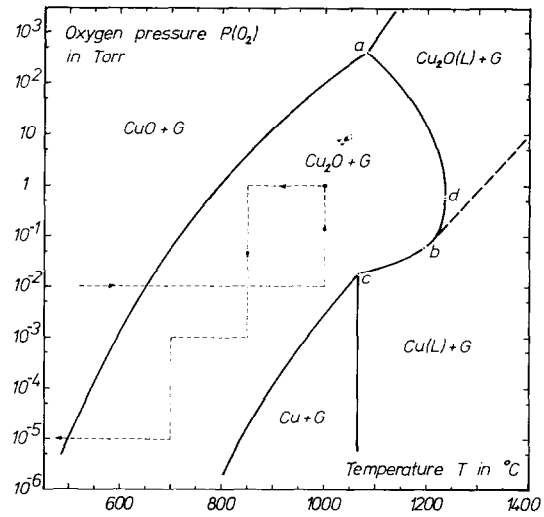

Fig. 1 Pressure versus temperature diagram in the copper–oxygen system. Invariant points: Cu_2O–CuO–eutectic a [$P(O_2)$ = 402 Torr, T = 1075 °C], Cu_2O monotectic b [$P(O_2)$ = 0.06 Torr, T = 1200 °C], Cu_2O–Cu–eutectic c [$P(O_2)$ = 0.018 Torr, T = 1065 °C]. Congruent Cu_2O melting point d [$P(O_2)$ = 0.6 Torr, T = 1235 °C]. Liquid phases are designated by a suffix L, gas phases by G. The annealing cycle (see part 4) is indicated by dashed lines.

at a magnification of 700×, Jusé and Kurtschatow[12]) observed small black needle-like crystals at 500× magnification. These crystals had usually combined to form V-shaped figures. Black spots near the centre of similar specimens were attributed by Grun[13]) to non-oxidized copper or to agglomerates of copper vacancies. Black inclusions visible to the naked eye, as well as smaller spike-shaped figures were reported by Goltzené et al.[14]) and identified as "negative crystals" produced by vacancy clustering. A closer look at their published micrographs also reveals the presence of tiny equiaxed inclusions. Annealing in vacuum has been reported either to eliminate these defects[12,14]), or to introduce new defects in the form of copper precipitates[15]). In melt-grown cuprous oxide, second phase inclusions have been variously identified as copper dendrites[5]), voids[6,7]) or cupric oxide particles[7]). Annealing at elevated temperatures and reduced oxygen pressures eliminated most of these defects[7]). Finally, transmission electron microscopical studies by Kužel et al.[16]) have produced evidence of submicron copper precipitation.

The aim of this work was to obtain cuprous oxide single crystals of controlled quality for mechanical deformation testing; due to the influence of a second phase on deformation properties, an attempt was made to identify the various types of microstructural defects and to investigate the conditions necessary for their appearance and for their elimination.

2. Single crystal growth

Polycrystalline starting material was prepared by total oxidation of copper rods of technical (99.9 % Cu) and of two high purity qualities (99.999 % and 99.999 % Cu) in air at 1045 °C. During oxidation a slight reaction between cuprous oxide and the platinum suspension wire was observed. In order to eliminate contamination, the position of the copper rods was chosen in such a manner that there was a large temperature gradient and resulting drop of temperature at the point of suspension. After cooling to ambient temperature in air, the surface layer of cuprix oxide was removed either by abrasion or by etching first with concentrated HCl and then with concentrated HNO_3[7]).

Liquid cuprous oxide attacks all known crucible materials, as shown by Zucker[5]). Single crystal growth was therefore carried out by a crucible-free method involving the floating zone technique associated with a bi-ellipsoid image furnace. The equipment utilized has been described in detail elsewhere[17]). The feed rod was suspended from a holder by a platinum wire and the lower polycrystalline rod fixed in a chuck. Growth was started by melting the tips of the two rods which were brought together in order to form a molten zone. In order to build up an ingot of about 10 to 15 mm diameter, the source rod had to be continually fed in. The top and bottom rods were rotated at 140 rpm in opposite directions in order to facilitate the stirring of the melt and to equalize the heat inflow. Crystal growth was usually carried out at the minimum seed withdrawal rate (1.2 cm/hr).

Seed crystals were obtained from the first coarse columnar-grained crystals by sectioning with a diamond saw. Several single crystals were grown from seeds with orientations ⟨100⟩, ⟨110⟩, ⟨111⟩ and ⟨211⟩. Single crystals were grown both in air and in controlled Ar/O_2 mixtures with $P(O_2) \approx 0.5$ and 10 Torr. The reduced oxygen partial pressures were chosen in order to reduce the temperature at which the phase boundary between Cu_2O and CuO was crossed (fig. 1), and thus to reduce the temperature dependent kinetics of CuO formation.

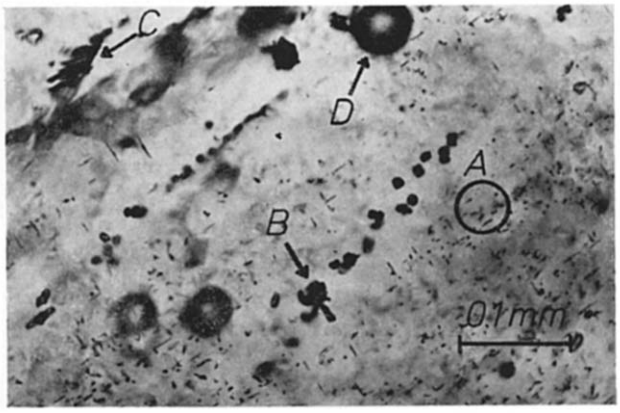

Fig. 2 Microstructure in optical transmission of polycrystalline cuprous oxide obtained by total oxidation of technically pure copper (air, $T = 1045\ ^{\circ}C$): polyhedral and spike-shaped cupric oxide (A), tentacled precipitate (B), dendritic cupric oxide (C), porosity (D).

3. Microstructure

The microstructures of Cu_2O crystals obtained by total oxidation of copper (totally oxidized material) and by growth from the melt were investigated by optical microscopy, electron microprobe analysis, and scanning electron microscopy. For optical microscopy, 0.1 to 0.3 mm thick disks were cut with an Isomet low speed diamond saw and polished mechanically, first on 600 grade abrasive paper and then with 5 μm diamond paste. The finished disks were transparent to red light, and a non-destructive observation in depth was possible.

3.1. Totally oxidized material

The totally oxidized material was quite porous. Two distinct regions were observed: in an outer layer of columnar grains fine pores were mainly distributed along grain boundaries, whereas in a central region of smaller equiaxed grains large cavities had formed. The grain structure was revealed either by the different reflecting properties of the variously oriented grains after abrasion, or by etching in a solution of 50% H_3PO_4, 30% H_2SO_4 and 20% HNO_3 at room temperature for 30 sec[18]).

A typical micrograph of the totally oxidized material shows a great variety of inclusions, fig. 2. These were identified as pores, dendritic CuO along columnar grain boundaries, polyhedral CuO precipitates and precipitate clusters within the grains. The cupric oxide precipitates were identified by X-ray microprobe analysis. Their shape was revealed by a technique of selective etching of the cuprous oxide matrix (1 part HNO_3 to 9 parts H_3PO_4 at room temperature gives etching rates of 10 μm/min). It could be shown that the majority of the pores was lined with a thin film of cupric oxide, fig. 3. These interior shells of CuO were formed in the same manner as the surface film of CuO: oxygen gas trapped in pores during oxidation interacted with the matrix Cu_2O when samples were cooled into the CuO stability region, see fig. 1. The fact that CuO dendrites were only found near the surface of totally oxidized specimens points to their formation due to a higher concentration of oxygen trapped during cooling along exterior grain boundaries, and not to a preferred precipitation at grain boundaries as such. Polyhedric CuO and precipitate clusters within the grains had presumably formed in a solid-state reaction during cooling as a result of copper vacancy agglomeration. In the notation of Kröger and Vink[19]) this can be written as a quasi-chemical reaction:

$$V_{Cu}^{Cu_2O} + Cu_{Cu}^{Cu_2O} + O_O^{Cu_2O} \rightarrow Cu_{Cu}^{CuO} + O_O^{CuO}. \qquad (2)$$

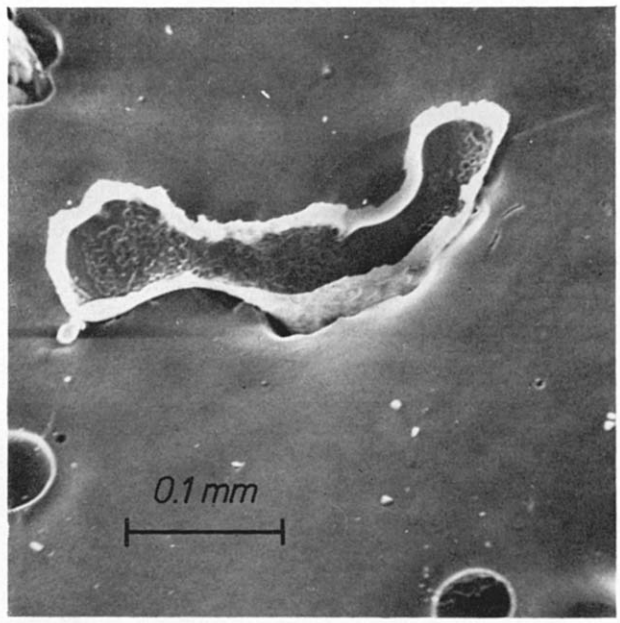

Fig. 3. Scanning electron micrograph of totally oxidized material. The lining of a pore with a cupric oxide skin is revealed by selective etching of the cuprous oxide matrix after sectioning.

3.2. Melt-grown Cu_2O

Single crystals of cuprous oxide grown from totally oxidized copper starting material were typically 12 mm

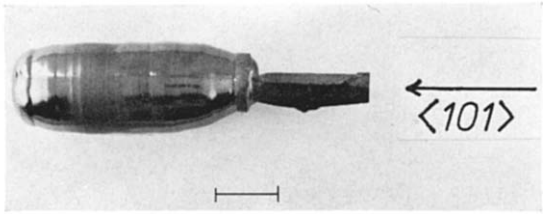

Fig. 4. A cuprous oxide single crystal grown from totally oxidized starting material in an Ar/O_2 atmosphere with $P(O_2) \approx$ 0.5 Torr and at a solidification rate of 1.2 cm/hr (marker = 1 cm).

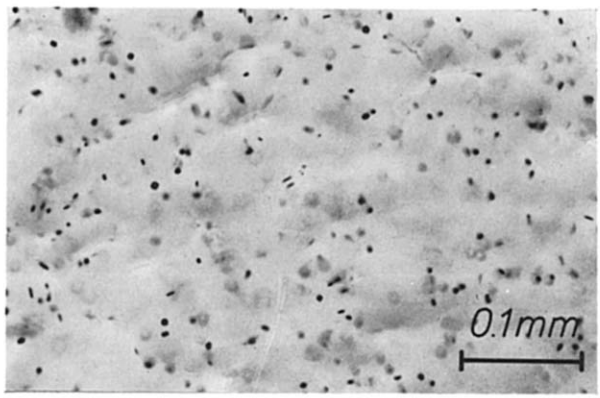

(a)

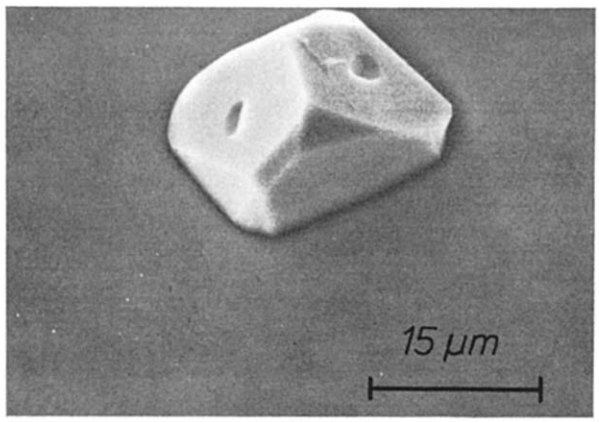

(b)

Fig. 5. Polyhedral cupric oxide precipitates in a melt-grown cuprous oxide single crystal (transversal section, near the surface); (a) optical transmission, (b) scanning micrograph after a selective etch of the matrix.

in diameter and 3.5 cm long, fig. 4. The morphology of precipitates was very similar to that found in the totally oxidized feed rods, although the number and distribution of inclusions differed considerably. Several experimental parameters were varied in order to find the optimum conditions for single crystal growth and perfection. The most pronounced influence on crystal perfection was that of the atmosphere during growth. Growth in air led to a very high precipitate density and to the formation of a CuO/Cu_2O eutectic at the end of the crystals. When the growth was polycrystalline, a dendrite network was formed along grain boundaries. In the crystals grown under a reduced $P(O_2)$ of 10 and 0.5 Torr the amount, if not the variety, of second phase precipitates was greatly diminished.

Several regions could be distinguished by their particular microstructure. At the bottom of the crystal near the surface cuprix oxide had usually precipitated as small polyhedrons, fig. 5. Towards the crystal axis large tentacle precipitates were visible. It was frequently observed that the tentacles of the complex precipitates were partly transparent, fig. 6a. This had previously led to their identification as pores[11]). In fact investigation of these inclusions by the selective etching technique and microprobe analysis clearly showed them to be a complex of cupric oxide precipitates and cavities, fig. 6b. In contrast to the facetted surface of the polyhedral precipitates (fig. 5), the surfaces of the group of precipitates forming a complex were more rounded with a concave irregular interface marking the original bubble/cuprix oxide boundary. The distribution of polyhedral CuO near the surface and tentacled precipitates near the crystal axis continued up to the top of the crystals. In the last few millimetres to solidify, a cellular structure of polyhedral precipitates appeared, with a larger cell diameter at the crystal centre than near the outer surface. The immediate surface region was always precipitate-free. In longitudinal sections of single crystals a periodic modulation of the precipitate density in the growth direction was observed (wave length about 0.5 mm). This coarse banding could be correlated with the feed-in cadence of the totally oxidized source material.

A mass spectrocopic analysis of the central portions of crystals grown from starting materials obtained from technically pure and from high purity copper showed no significant difference in the main impurity contents (Ag, Mg, Fe, Mn, Si). The general features of precipitation were not influenced by the purity of the original copper, with the exception that cells were not formed with high purity starting material. A variation of the speed of solidification from 1.2 cm/hr to higher values had a deleterious effect: At speeds of 5 cm/hr macroscopic pores were observed which served as nucleation

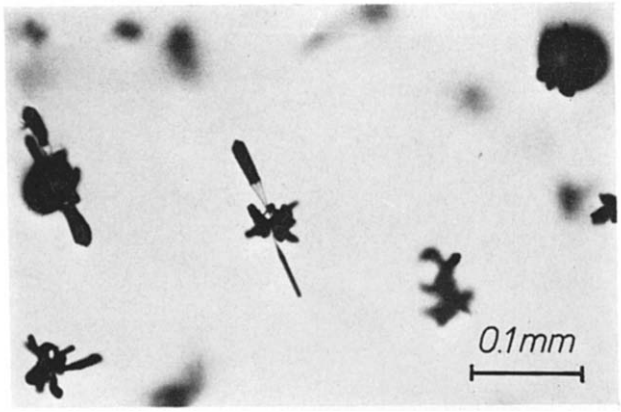

(a)

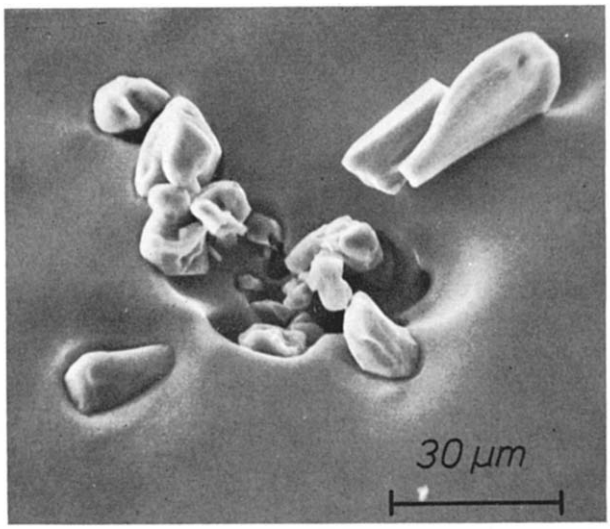

(b)

Fig. 6. Tentacled precipitates in a cuprous oxide single crystal grown from the melt (transversal section, near the core): partly transparent tentacle in optical transmission (a) and scanning micrograph after a selective etch of the matrix, revealing a complex of cupric oxide precipitation and porosity (b).

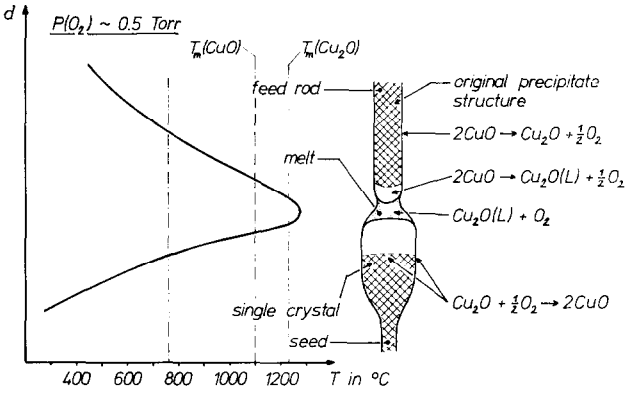

Fig. 7. Schematic representation of single crystal growth in an arc-image furnace. The feed rod and growing single crystal are lowered though a temperature profile (left) at the solidification rate R. During heating, melting and cooling in an atmosphere with reduced $P(O_2) \approx 0.5$ Torr, various phase changes and reactions occur (right). Regions of solid cuprous oxide with cupric oxide precipitation are indicated by hatching, the liquid zone by dots (see text for further details).

points for polycrystalline growth. The spread of orientation in single crystals as determined from back-reflection X-ray Laue spots grew from less than $\pm 0.5°$ for solidification rates of 1.2 cm/hr to $\pm 2°$ for rates of 5 cm/hr. Attempts were made ro reveal the dislocation density of solidified samples by etch-pitting on (111) planes in a solution of 12% copper nitrate and 10% nitric acid[20]). Although grain and subgrain boundaries were revealed, the density of etch pits within grains did not give reproducible results.

3.3. Discussion of the growth process

A better understanding of the formation and distribution of all the defects observed in the single crystal cuprous oxide requires a careful look at the process of melting and solidification. The feed rod with its precipitate structure, the molten zone and the solidified single crystal were subjected to the temperature profile shown schematically in fig. 7. At some distance above the molten zone, the precipitate structure of the feed rod remained unchanged. Where the temperature exceeded about 700 °C, a film of CuO started to form on the surface. In an atmosphere of reduced oxygen partial pressure [$P(O_2) \approx 0.5$ Torr] this surface film dissolved again at about 760 °C, and was therefore not introduced into the melt. The CuO precipitates within the bulk of the feed rod were not decomposed so quickly. It is likely that they were melted when the CuO liquidus was reached at about 1100 °C and then introduced into the cuprous oxide rich melt which formed at 1220 °C. As a result of the incorporation of cupric oxide, the melt became oxygen-rich. A further contribution to the liquid was brought by the porosity of the feed rod, most probably in form of further oxygen gas trapped during the original oxidation of copper to cuprous oxide. In spite of the vigorous stirring of the melt, it appears that only the gas near the surface managed to excape.

During solidification, minute bubbles of oxygen were trapped in the central region of the crystal. Below about 760 °C, cupric oxide began to form again where there

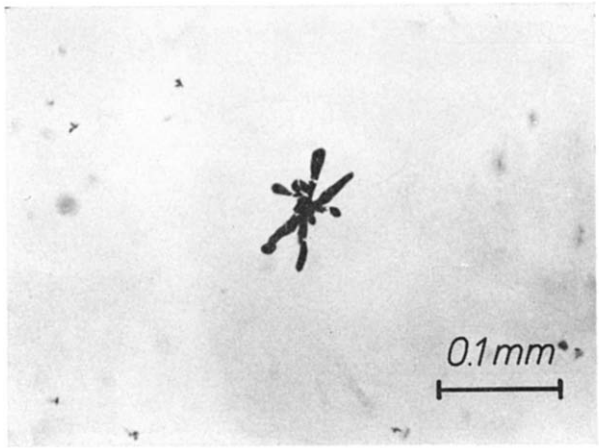

Fig. 8. Beginning dissolution of a complex precipitate after an intermediate anneal at 1000 °C and $P(O_2) = 1$ Torr (optical transmission). All polyhedral cupric oxide precipitates have disappeared, at the same time star-shaped inclusions have formed.

was a supply of oxygen, i.e. at outer and inner interfaces between oxygen and cuprous oxide: a very thin film of cupric oxide was formed on the crystal surface and the interface between trapped bubbles and the bulk material. This reaction continued either until equilibrium $P(O_2)$ was reached in the bubbles or the kinetics of the oxidation reaction became too slow. The complex tentacle-shaped precipitates were nucleated by this reaction at inner surfaces. The precipitation of polyhedral cupric oxide and any further precipitate growth in the stability field of CuO was likely to be by the mechanism of internal aggregation of copper vacancies proposed previously in eq. (2).

4. Annealing procedure and further discussion

The annealing procedure utilized in this study was very similar to that described by Brower and Parker[7]). The cuprous oxide crystals to be treated were placed on platinum foil and enclosed in a controlled atmosphere furnace. The crystals were heated in air to temperatures varying from 900 to 1050 °C in a total pressure of 0.1 Torr. Air was introduced into the chamber by a needle valve and the anneal was continued under dynamic conditions with a partial oxygen pressure of 1 Torr. At the end of the treatment, temperature and oxygen partial pressure were reduced in such a way that the crystals were always maintained within the region of stability of cuprous oxide, fig. 1. The Cu_2O/CuO phase boundary was crossed at temperatures varying from 400 to 500 °C, i.e. in conditions where the kinetics of

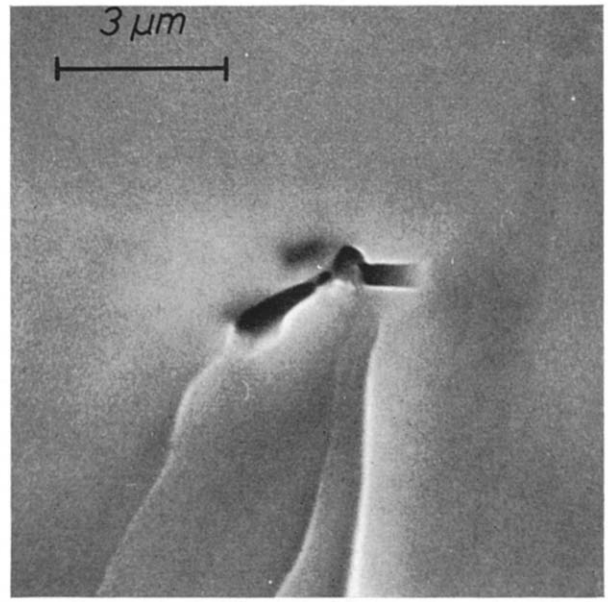

Fig. 9. Scanning electron micrograph of a cleaved cuprous oxide single crystal annealed at 1000 °C and $P(O_2) = 1$ Torr. River markings originate at a star-shaped pore.

CuO formation are negligible. After this treatment, samples had practically 100 % of the density calculated from the lattice parameter and composition ($\rho_{theor} = 6.10$ g/cm^3).

The annealing sequence could be divided into several stages. After an anneal of several hours, all polyhedral and disk-shaped precipitates had disappeared. At the same time star-shaped inclusions had been formed throughout the specimen except within the immediate vicinity of complex precipitates. After further annealing, the complex precipitates nearest to the crystal surface had started to dissolve, fig. 8. With continued annealing, the zone free of complex precipitates extended towards the centre of the specimens. Finally all complex precipitates were eliminated, and only the star-shaped inclusions remained.

In order to find out the nature of the stars, specimens of annealed cuprous oxide were cooled to liquid nitrogen temperature and fractured in a brittle manner. The fracture surface sometimes cut through the star-shaped inclusions, fig. 9, and showed them to be pores.

The depth of the zone free of cuprix oxide after varying times of anneal at 1000 °C and $P(O_2) = 1$ Torr was measured and the kinetics compared with those of oxidation of copper under similar conditions, fig. 10. It can be seen that there is quite a good agreement between

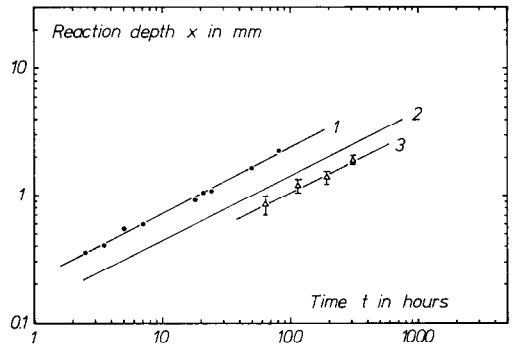

Fig. 10. Reaction depth x as a function of time for various phase reactions in the system copper–oxygen: (1) oxidation of Cu to Cu_2O at 1045 °C in air; (2) oxidation of Cu to Cu_2O at 1000 °C and $P(O_2) = 1$ Torr, calculated from parabolic rate constants (ref. 20 and 21); (3) dissolution of complex CuO–O_2 precipitates in cuprous oxide at 1000 °C and $P(O_2) = 1$ Torr.

the curves for oxidation of copper to cuprous oxide and dissolution of precipitate complexes (reduction of cuprix oxide to cuprous oxide). The time-dependence of the dissolution process

$$x = \text{const.} \times t^{0.5} \tag{3}$$

(x = mean thickness of cupric oxide free zone), and the fact that the dissolution of precipitate complexes originates at the specimen surface, point to a reaction where copper vacancies are emitted by the cupric oxide and subsequently migrate to the surface. This is the reverse reaction of eq. (2). The flux of vacancies away from the precipitates reduces the copper vacancy concentration in the immediate precipitate vicinity and allows the dissolution to continue. It is possible that the preferred dissolution of polyhedral precipitates is due to the same process with the exception that the copper vacancies migrate to the inner surfaces supplied by the bubbles which are a part of the complex precipitates. The shorter migration paths would explain the reduced reaction times. The small stars which remained even after prolonged anneals could have been formed either by precipitation of copper vacancies during cooling, or Ostwald ripening of tiny oxygen gas bubbles released during solidification.

A further effect of the high temperature anneal was the rearrangement of dislocations introduced into the matrix during the solidification process. These statistically distributed dislocations became mobile at high temperature and formed a polygonized structure. This structure was visible on the specimen surface (thermal etching) and also in the bulk due to a decoration of cell walls by the star-shaped pores.

In view of the beneficial effect of a high-temperature anneal in the stability region of cuprous oxide, several growth runs were conducted under controlled atmosphere [$P(O_2) \approx 0.5$ Torr] and with annealed feed rods. The most striking difference was the complete absence of complex precipitates, although the polyhedral cupric oxide particles were observed to form clusters. In general the precipitates were more homogeneously distributed and less dense when annealed starting material was utilized. These results are due to the reduced amount of cuprix oxide fed into the melt and to the concomitant reduction of oxygen excess in the liquid zone.

5. Summary

Due to the common features in the elaboration of cuprous oxide by total oxidation of copper and by melt growth (formation in the stability region of Cu_2O, post-solidification precipitation of CuO during cooling), there is a marked similarity of the resulting precipitate structures at ambient conditions.

Large single crystals of cuprous oxide have been grown from the melt, but the process of fabrication introduced a number of inherent defects such as cupric oxide precipitates and oxygen gas bubbles. The optimum conditions for crystal growth and treatment were found to be the following:

(1) Pre-growth anneal of feed material (1000 °C, 1 Torr oxygen pressure). This reduces the amount of cupric oxide introduced into the melt, diminishes the amount of post-solidification precipitation of cupric oxide, and eliminates complex precipitates.

(2) Growth under reduced oxygen partial pressure ($\approx$ 0.5 Torr). This further reduces the amount of cupric oxide precipitation.

(3) Post-growth anneal (1000 °C, 1 Torr oxygen pressure). All cupric oxide precipitates are eliminated. The remaining microscopic star-shaped pores are most probably filled with oxygen. Their number depends on the original amount of precipitation.

Oriented samples have been cut from single crystals grown and treated in this fashion. The results of deformation measurements and of an electron microscopical study will be published when they become available.

Acknowledgements

It is a pleasure to thank Professor J. Philibert for his interest in this work and for critical reading of the manuscript. Discussions with Professor D. Trivich have been particularly rewarding. One of us (R.D.S.W.) wishes to thank the Deutsche Forschungsgemeinschaft for the award of a Research Fellowship, another (M.M.C.) the French Ministry of Foreign Affairs for a grant accorded under the agreement of technical co-operation between France and Spain.

References

1) G. Blankenburg and K. Kassel, Ann. Physik [6] **10** (1952) 201.
2) R. S. Toth, R. Killeson and D. Trivich, J. Appl. Phys. **31** (1960) 117.
3) Y. Ebisuzaki, J. Appl. Phys. **32** (1961) 2027.
4) A. Kinoshita and T. Nakano, Japan. J. Appl. Phys. **6** (1967) 656.
5) R. S. Zucker, J. Electrochem. Soc. **112** (1965) 417.
6) D. Trivich and G. P. Pollack, J. Electrochem. Soc. **117** (1970) 344.
7) W. S. Brower and H. S. Parker, J. Crystal Growth **8** (1971) 227.
8) M. O'Keeffe and W. J. Moore, J. Chem. Phys. **36** (1962) 3009.
9) M. Hansen and K. Anderko, *Constitution of Binary Alloys* (McGraw-Hill, New York, 1958).
10) G. Eriksson, Acta Polytechn. Scand. Ch. **99**, II (1971) 20.
11) O. Böttger, Ann. Physik [6] **10** (1952) 232.
12) W. P. Jusé and B. W. Kurtschatow, Physik. Z. Sowjetunion **2** (1932) 453.
13) J. B. Grun, Rev. d'Optique **41** (1962) 439
14) A. Goltzené, C. Schwab and S. Nikitine, Compt. Rend. (Paris) C **265** (1967) 1360.
15) E. Engelhard, Ann. Physik [5] **17** (1933) 501.
16) R. Kužel, C. D. Cann, S. S. Sheinin and F. L. Weichmann, Can. J. Phys. **48** (1970) 2657.
17) A. Revcolevschi, Rev. Intern. Hautes Tempér. Réfract. **7** (1970) 73.
18) R. Collongues and R. Sifferlen, J. Chim. Phys. **53** (1956) 803.
19) F. A. Kröger and H. J. Vink, in: *Solid State Physics*, Vol. 3, Eds. F. Seitz and D. Turnbull (Academic Press, New York, 1956) p. 307.
20) A. I. Andrievskii and G. F. Mocharnyuk, Kristallografiya **8** (1963) 120.
21) C. Wagner and K. Grünewald, Z. Physik. Chem. B **40** (1938) 455.
22) J. P. Baur, D. W. Bridges and W. M. Fassell jr., J. Electrochem. Soc. **103** (1956) 273.